Signal quality and compactness of a dual-accelerometer system for gyro-free human motion analysis

Article

Published Version

Open access

Signal Quality and Compactness of a Dual-Accelerometer System for Gyro-Free Human Motion Analysis

Emma Villeneuve, William Harwin, William Holderbaum, R. Simon Sherratt, *Fellow, IEEE*, and Ruth White

Abstract—There is a growing interest in measuring human activities via worn inertial sensors, and situating two accelerometers on a body segment allows accessing rotational kinematic information, at a significantly lower energy cost when compared with gyroscopes. However, the placement of sensors has not been widely considered in the literature. In practice, dual-accelerometer systems should be built as compact as possible to ensure long-term wearability. In this paper, the impact of sensor placement and nature of human activity on signal quality is quantified by individual and differential signal-to-noise ratios (SNRs). To do so, noise-free signals are described by a 2-D kinematic model of a body segment as a function of kinematic variables and sensor location on the segment. Measurements are modelled as kinematic signals disturbed by zero mean additive Gaussian noise. Depending on the accuracy needed, one can choose a minimal SNR to achieve, with such dual-accelerometer arrangement. We estimate SNR and minimal sensor separations for three data sets, two from the public domain and one collected for this paper. The data sets give arm motion profiles for reaching, inertial data collected during locomotion on a treadmill and during activities of daily life. With a dual-accelerometer arrangement, we show that it is possible to achieve a good differential SNR for the analysis of various human activities if the separation between the two sensors and their placement is well chosen.

Index Terms—Accelerometers, angular velocity, wearable sensors, signal to noise ratio, biomedical monitoring.

I. INTRODUCTION

INERTIAL Measurements Units (IMUs), which provide the orientation and motion of a moving body, are widely used within the biomedical community [1]. Interest in inertial sensors has grown due to their low price, compactness and accessibility to the general public. They are often used to estimate angles of human limbs, particularly lower limb angles for gait analysis [2]–[10].

TABLE I
DISTANCES ℓ_i OF THE i^{TH} ACCELEROMETER FROM THE JOINT, IN LITERATURE. DISTANCES $d = \ell_2 - \ell_1$ BETWEEN ACCELEROMETERS

Ref.	Type of Motion	Accelerometer Placement	ℓ_1 [m]	ℓ_2 [m]	d [m]
[3]	Walking	Thigh	$\simeq 0.15$	$\simeq 0.5$	$\simeq 0.25$
		Shank	$\simeq 0.15$	$\simeq 0.40$	$\simeq 0.25$
[18]	Walking	Thigh and shank	n.a.	n.a.	0.14
[5]	Walking	Thigh, shank and foot	n.a.	n.a.	0.055
[2]	Walking	Thigh	0.10	0.19	0.09
			0.14	0.19	0.05
			0.17	0.19	0.02
[19]	Undetermined	Robot arm	0.727	0.867	0.14
			0.584	0.867	0.283
[15]	Oscillation	Pendulum	10 acc. on 40 cm	0.4	0.04

Angles can be computed from accelerometer data, however for gait analysis angular velocities are also beneficial [11]. These features are useful for activity classification, especially when combined with acceleration intensity [12]. Although gyroscopes can directly measure angular velocity, they can consume 1000 times more current than accelerometers.[1] Therefore they are less appropriate for a long term residential monitoring system where low power is crucial.

The angular acceleration can be estimated from the difference between the signals from two 2D accelerometers [2], [5]. The angular velocity is recoverable from either the angular acceleration term or the squared velocity term. The acceleration term can be integrated [5], alternatively the squared angular velocity term can be used as a computation of the absolute value of the velocity [2], with the sign estimated from other sources [15]. A pair or an array of accelerometers can also be used to estimate angle without integration in order to remove the body linear acceleration [3], [15].

A key point of this study is to find a compromise between the compactness of a dual-accelerometer, which depends on their separating distance, and a good measurement quality measured by a high Signal-To-Noise-Ratio (SNR). Table I presents some locations of pairs of accelerometers in the literature. There are large variations of the distances between accelerometers for the same motion (walking) and the same

---

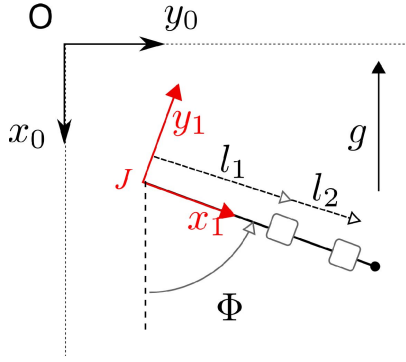[1] The normal operating current is 1.8 μA for the ADXL362 accelerometer [13] and 3600 μA for the MPU-6050 gyroscope [14].

Fig. 1.   Body segment model. The inertial reference coordinate system is $(O, \boldsymbol{x}_0, \boldsymbol{y}_0)$. The system $(O, \boldsymbol{x}_1, \boldsymbol{y}_1)$ is attached to the body segment. Vector g is the gravity component, as measured by accelerometers.

limb (thigh), from 2 cm [2] to 25 cm [3]. However, the quality of angle estimation improves with the distance between accelerometers [2].

With the development of residential monitoring, the compactness of a measurement system is crucial for user acceptance. If both accelerometers are close enough, they can be encased in a single wearable system. This paper suggests metrics to quantify the impact of the sensor placement and separation on the signal quality. Choosing a minimum signal quality dictates a minimal sensor separation between a pair of accelerometers so that the difference between both accelerometer signals can be exploited.

Section II analyses the relationship between the performances of a dual-accelerometer system, the sensor placement and separation. In section III, performances are quantified in several cases of locomotion and activity. Three datasets including arm motion profiles [16], inertial data collected in a laboratory environment and inertial data collected in a house environment from the Opportunity dataset [17], provide the necessary motion features. Finally, sections IV and V focus on the sensor separation for a chosen minimal signal quality level in order to build a dual-accelerometer as compact as possible. Minimal separations are estimated using the same datasets for simple motions and daily activities.

II. SIGNAL QUALITY METRICS

A 2D kinematic model based on the sagittal plane is used to assess the performance of a dual-accelerometer system [2]–[5], [18]. This allows us to limit the dependencies of the SNR function.

A. 2D Kinematic Model of a Body Segment

The motion of a body segment in the sagittal plane can be described by the angle $\phi \in \,]-\pi \, ; \pi]$, angular velocity $\omega \in \mathbb{R}$ and angular acceleration $\alpha \in \mathbb{R}$ of this segment. The unknown kinematic variables are gathered in the following state-vector:

$$\boldsymbol{x} = [\phi, \omega, \alpha]^T. \qquad (1)$$

As can be seen in Fig. 1, the angle corresponds to the rotation between the reference system of coordinates $(O, \boldsymbol{x}_0, \boldsymbol{y}_0)$ and the local system $(O, \boldsymbol{x}_1, \boldsymbol{y}_1)$.

The measured acceleration of a point located on the body segment, written in the local coordinate system $(O, \boldsymbol{x}_1, \boldsymbol{y}_1)$ and relative to the reference system, is given by the following function $\boldsymbol{h}$:

$$\boldsymbol{h}(\boldsymbol{x}_t, \ell) = \boldsymbol{a}_{J,t}^1 + \begin{pmatrix} -\ell\omega_t^2 - g\cos\phi_t \\ \ell\alpha_t + g\sin\phi_t \end{pmatrix} \qquad (2)$$

where subscript t is the time index, $\boldsymbol{a}_J^1$ is the acceleration of point J which is the origin of the body segment, written in coordinate system {1}, ℓ the distance of the point from the joint J, and g the gravity component.

B. Statistical Observation Model

Accelerometers measure linear acceleration with an associated measurement noise that can be modelled as an additive zero mean Gaussian noise [15]. The measurements on the ith 2D accelerometer on the body segment are modelled by a statistical observation model:

$$\boldsymbol{z}(\boldsymbol{x}_t, \ell_i) = \boldsymbol{h}(\boldsymbol{x}_t, \ell_i) + v_t \quad \text{with } v_t \sim \mathcal{N}(\boldsymbol{0}, R) \qquad (3)$$

where $R \in \mathbb{R}^{2\times 2}$ is the covariance matrix of the Gaussian noise v_t [15]. If the noise on both axes have the same statistical properties and are independent as in [15], then the covariance matrix simplifies as $R = \sigma^2 I_2$ with I_2 the identity matrix of $\mathbb{R}^{2\times 2}$ and $\sigma \in \mathbb{R}^+$ the standard deviation. It is reasonable to assume noise is independent as each accelerometer creates its own thermal noise.

C. Difference Between 2 Accelerometers

Two 2D accelerometers are located on the body segment at ℓ_1 and ℓ_2 from the joint. Assuming the noise on both accelerometers is independent [15], the difference between two accelerometer signals is defined as:

$$\boldsymbol{z}_\delta(\boldsymbol{x}_t, \ell_1, \ell_2) = \boldsymbol{z}(\boldsymbol{x}_t, \ell_2) - \boldsymbol{z}(\boldsymbol{x}_t, \ell_1) \qquad (4)$$
$$= \boldsymbol{h}_\delta(\boldsymbol{x}_t, \ell_1, \ell_2) + \boldsymbol{n}_t \qquad (5)$$

with

$$\boldsymbol{h}_\delta(\boldsymbol{x}_t, \ell_1, \ell_2) = \boldsymbol{h}(\boldsymbol{x}_t, \ell_2) - \boldsymbol{h}(\boldsymbol{x}_t, \ell_1) \qquad (6)$$
$$= \begin{pmatrix} -(\ell_2 - \ell_1)\omega_t^2 \\ (\ell_2 - \ell_1)\alpha_t \end{pmatrix} \qquad (7)$$
$$\boldsymbol{n}_t \sim \mathcal{N}(\boldsymbol{0}, 2R) \qquad (8)$$

The difference between two observations only depends on the sensor separation $\ell_2 - \ell_1$, and angular kinematics ω_t and α_t. It is subject to greater noise when compared to the individual observation, as the cumulated covariance matrix is $2R$. Note that if both sensors are disturbed by an identical noise due to external factors such as skin motion, then this perturbation is removed by computing the difference of signals.

D. Signal-to-Noise Ratio

The SNR is defined by the ratio of the signal energy (if the energy is finite) by the noise energy. Let's consider a signal acquired during an interval $[0; T]$. Then, the signal energy is given by the integration of the instantaneous power P during this interval. Assuming, the noise variance σ^2 is constant

over time, then the SNR of the 2D accelerometer signal on both axes reads as follows:

$$SNR = \frac{\int_{[0;T]} P(t)dt}{2T\sigma^2} \qquad (9)$$

The SNR can be considered good when it is above 1 (0 dB), which means there is more signal than noise. However, applications such as kinematic estimation or classification do not require the same level of SNR.

1) Instantaneous Power: The instantaneous power $P(\boldsymbol{x}_t, \ell)$ of the noise-free signal of one accelerometer is defined as the squared 2-norm of the vector-signal at each time t:

$$P(\boldsymbol{x}_t, \ell) = ||\boldsymbol{h}(\boldsymbol{x}_t, \ell)||_2^2 \qquad (10)$$
$$= \ell^2(\omega_t^4 + \alpha_t^2) + g^2$$
$$+ 2\ell g(\omega_t^2 \cos\phi_t + \alpha_t \sin\phi_t) \qquad (11)$$

The instantaneous power of the noise-free difference signal between two 2D accelerometer located at at ℓ_1 and ℓ_2 is given by the squared 2-norm of the difference signal:

$$P_\delta(\boldsymbol{x}_t, \ell_1, \ell_2) = ||\boldsymbol{h}_\delta(\boldsymbol{x}_t, \ell_1, \ell_2)||_2^2 \qquad (12)$$
$$= (\ell_2 - \ell_1)^2(\omega_t^4 + \alpha_t^2) \qquad (13)$$

Hereafter P and P_δ are called individual and differential instantaneous power.

2) Individual SNR:

$$SNR = \frac{\int_{[0;T]} P_1(\boldsymbol{x}_t, \ell)dt}{2T\sigma^2} \qquad (14)$$
$$= \frac{\ell^2(\overline{\omega^4} + \overline{\alpha^2})}{2\sigma^2} + \frac{g^2}{2\sigma^2} \qquad (15)$$

with

- $\overline{\omega^4}$ is the average power of ω_t^2: $\overline{\omega^4} = \frac{1}{T}\int_{[0;T]} \omega_t^4 dt$
- $\overline{\alpha^2}$ is the average power of α_t: $\overline{\alpha^2} = \frac{1}{T}\int_{[0;T]} \alpha_t^2 dt$

According to equation (15), the individual SNR increases with the sensor distance ℓ to the joint.

3) Differential SNR: The differential SNR is given by the ratio of the energy of the difference signal, by the energy of the noise of variance $2\sigma^2$:

$$SNR_\delta = \frac{\int_{[0;T]} P_\delta(\boldsymbol{x}_t, \ell_1, \ell_2)dt}{4T\sigma^2} \qquad (16)$$
$$= \frac{(\ell_2 - \ell_1)^2(\overline{\omega^4} + \overline{\alpha^2})}{4\sigma^2} \qquad (17)$$

According to equation (17), the differential SNR increases with the distance $d = \ell_2 - \ell_1$ between both accelerometers. Note that the sampling rate does not affect both individual and differential SNR, assuming it is sufficient to correctly capture human motions.

III. PERFORMANCE ANALYSIS

Three datasets were used in this study, two from the public domain and one collected for this paper. The datasets give arm motion profiles for reaching, inertial data collected during locomotion on a treadmill, and inertial measurements during activities of daily life.
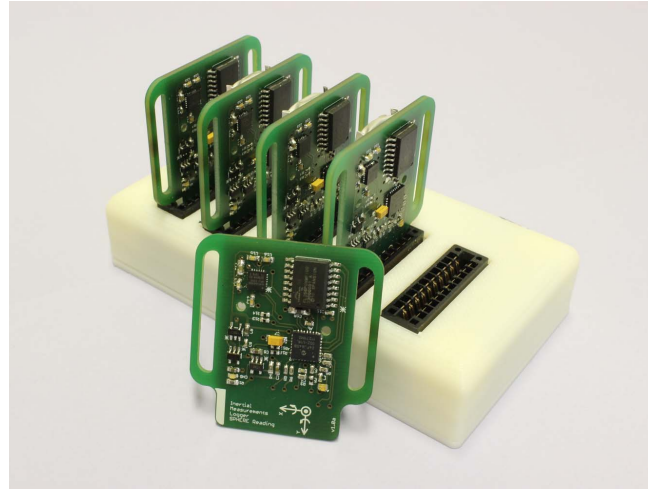

Fig. 2. Inertial sensor board equipped with a 3D accelerometer and a 3D gyroscope, used in the Controlled Locomotion Experiment (Section III-B).

A. Arm Motion Profile (Nagasaki Dataset)

1) Description: The Nagasaki dataset [16] is a publicly available data source that provides the angular velocity and acceleration profiles for arm motion, when reaching a target. Four seated male subjects, aged from 31 to 49, were asked to point to a target at different angles [20, 30, 40, 50, 60] degrees from the starting position, and at different speeds which were defined as slow, intermediate and ballistic. The instantaneous angle of the hand was measured by a goniometer, activated through a specially made handle, and recorded at 1 kHz. Each configuration of amplitude and speed was collected ten times, for each subject. The study provides the average angular displacement, the duration and the average acceleration.

2) Data Processing: Using the arm motion profiles [16], the average angular velocity $\overline{\omega}$ is estimated by the ratio of the average angular displacement and the duration. From $\overline{\omega}$ and the measured average acceleration $\overline{\alpha}$ [16], the motion features $\overline{\omega^4}$ and $\overline{\alpha^2}$ are computed for each angle and each speed, assuming that $\overline{\omega}$ and $\overline{\alpha}$ are constant over time. This approximation allows the computation of the motion features without knowing the instantaneous velocity and acceleration for each time sample. The corresponding differential SNR is then computed using equation 17, for a target at 40 degrees and a noise standard deviation $\sigma = 6$ mg. This level of noise was measured using the accelerometer of type ADXL362. Results are given in Figure 4.

B. Controlled Locomotion (Dataset Collected for This Study)

1) Description: In order to measure reliable motion features for locomotion, inertial data were collected from one healthy female subject aged 30, walking or slowly running on a treadmill at a constant speed of 2.5 km/h or 6 km/h, during during 3 minutes. Data were captured at 50 Hz using three inertial sensor boards (Figure 2) developed by the SPHERE project, relying on 3D accelerometers ADXL362 and 3D gyroscopes MPU6050. Sensors were located at distal ends of the left upper arm, forearm, thigh and shank. They were

attached with Velcro straps and orientated so that the plane formed by axes X and Y was parallel to the sagittal plane. The longer duration of the collected data allows a better accuracy on the averaging for motion features $\overline{\omega^4}$ and $\overline{\alpha^2}$.

2) Data Processing: Angular velocity from the gyroscope on the main rotation axis allows $\overline{\omega^4}$ to be computed directly. The angular acceleration is derived by numerical differentiation and provides $\overline{\alpha^2}$. Note that the estimation of $\overline{\omega^4}$ and $\overline{\alpha^2}$ is robust against noise, as it was realised from 9000 samples. Using these two features, one can compute the differential SNR using the Equation 17. Results are given in Figure 4.

C. Daily Activities (Opportunity Dataset)

1) Description: A subset of the publicly available data published as the Opportunity Activity Recognition Dataset [17], is used in this paper. It contains inertial data collected on four subjects. Four Xsens IMU (accelerometers and gyroscopes) were located on left and right upper and forearms, and attached to a jacket by straps. Subjects were asked to perform a series of daily morning activities in a residential environment, each series iterated five times. Thanks to annotation, inertial data are associated with locomotion labels (stand, walk, sit, lie) and high-level activity labels (relaxing, coffee time, early morning, cleanup, sandwich time).

2) Data Processing: We selected gyroscope measurements on the main rotation axis and associated to the 'walking' label or activity labels. Data were filtered by a low-pass filter in order to reduce noise. Motion features $\overline{\omega^4}$ and $\overline{\alpha^2}$ were computed using the resulting filtered data and averaged on data from four subjects and five repetitions. Differential SNR were derived from the equation 17, with the same level of noise $\sigma = 6$ mg. Results are given in Figure 4.

D. Impact of Sensor Placement and Separation on SNR

According to equations 15 and 17, the individual SNR increases with the squared distance of the sensor from the joint, and the differential SNR increases with the squared sensor separation. Hence, there is a trade-off between the signal quality of a dual-accelerometer system and its compactness.

Figure 3 (a) shows the individual SNR of the first sensor as a function of its location $\ell_1 = \ell_2 - d$. Based on the controlled locomotion dataset III-B collected for this study, the individual SNR varies between 41 and 46 dB for all sensor placements on the body, for walking and running. So in practice, the individual SNR is always very high. In the following, the study focuses on the differential SNR.

Figure 3 (b) shows the differential SNR as a function of the separation between accelerometers, for several sensor placements, during walking and running on a treadmill (Controlled Locomotion experiment III-B). The differential SNR seems sensitive to sensor placement, and for walking it increases as the sensor is located lower on the body. For instance, there is a gap of +15 dB between SNR on the upper arm and on the shank during walking, and a gap of +7 dB during running. This result is logical since lower limbs are longer than upper limbs so they have higher accelerations. As evident in Figure 3 (b), a separation of a few centimetres is necessary
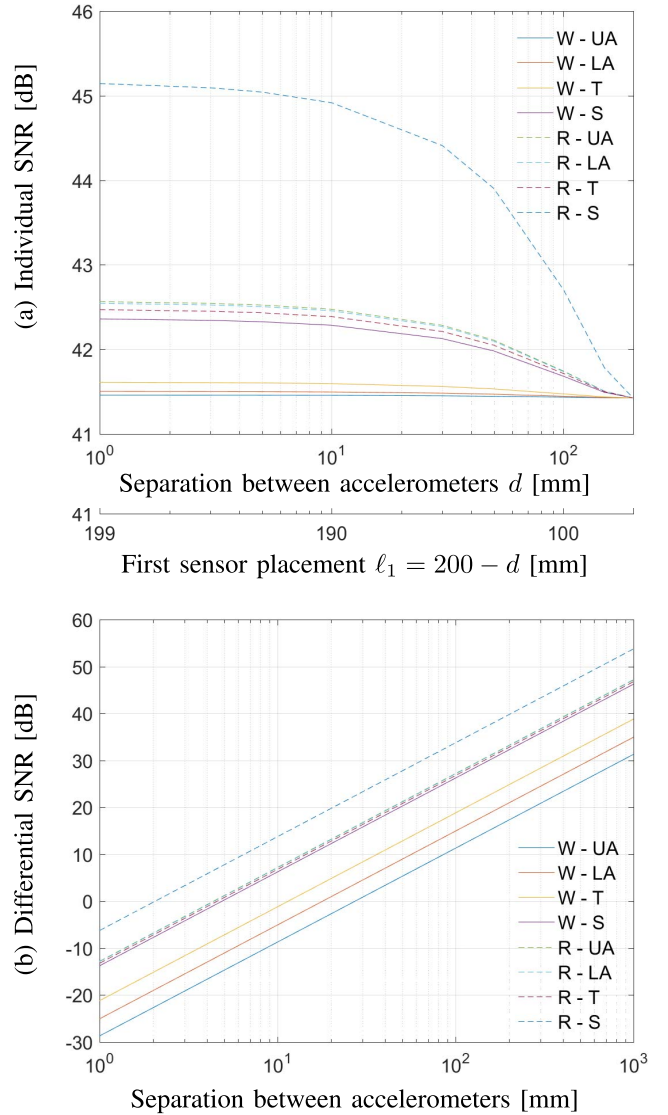

Fig. 3. Signal-to-Noise-Ratio as a function of the sensor separation and placement. (a) Individual SNR of the first accelerometer. (b) Differential SNR of two accelerometers. Computed for two activities (W: Walking, R: Running) and four sensor placements (UA: Upper Arm, LA: Lower Arm, T: Thigh and S: Shank). Computed from the controlled locomotion dataset of Section III-B.

to get a differential SNR above 0 dB on the arms and thigh during walking. But only a few millimetres are necessary for running and for a shank sensor during walking. There is a gap of +20 dB between the differential SNR values for sensor separations of 3 mm and 3 cm, for a given activity and sensor placement. Both sensor separations are feasible, but resulting signal qualities quantified by the differential SNR are dramatically different. So, not only the SNR depends on sensor placement but also strongly on the sensor separation and on the activity.

E. Impact of Activities on SNR

Figure 4 shows the values of the differential SNR computed for all motion atoms and activities in the Nagasaki dataset [16], the Controlled Locomotion dataset (III-B) and the Opportunity dataset [17], for a fixed sensor separation of 3 cm. In the case
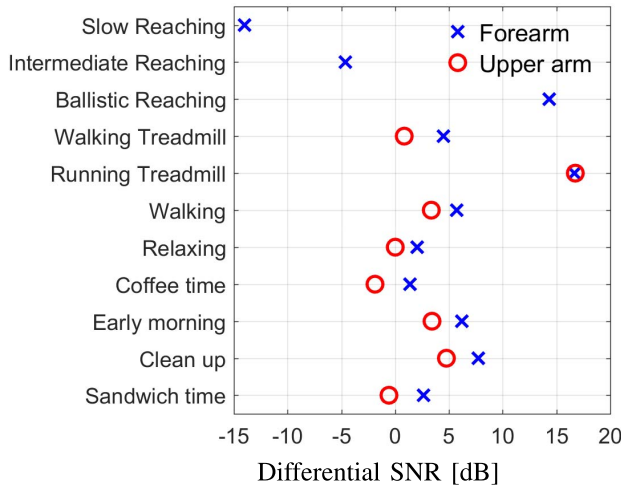
Fig. 4. Differential Signal-to-Noise-Ratio, for several motions and activities. Activities no.1-3 are reaching to target at 40 degrees [16]; activities no. 6-11 are extracted from the Opportunity dataset [17].

of daily activities from the Opportunity dataset, the differential SNR varies between 1 and 8 dB for forearm sensors (cf. Figure 4). This is a small variation because activities are mixtures of motion atoms at various speeds and in different proportions.

Overall, there is a difference of 30 dB between the lowest SNR realized during 'slow reaching' (-14 dB) and the highest SNR achieved during 'ballistic reaching' (14 dB) and 'running on a treadmill' (17 dB). This strong variation, due to the different speeds of motion, confirms that the differential SNR depends more on the nature of activity than on the sensor placement on the body. However, 'slow reaching' and 'ballistic reaching' are extreme motions that are unlikely to occur often in daily life. Figure 4 also shows that differential SNR on the upper arm and forearm are quite close for all motions and activities.

So it is possible to achieve a good differential SNR for the analysis of various human activities if the sensor separation and placement are well chosen.

IV. SENSOR SEPARATION FOR A COMPACT DUAL ACCELEROMETER

Section III has highlighted the impact of the sensor separation and placement and the user activity on the quality of signals. In practice, a dual-accelerometer system should be designed as small as possible to ensure the user can wear it. Depending on motion analysis methods, a minimal SNR can be chosen to achieve a target accuracy. In this section, we analyse the sensor separation for a chosen SNR.

A. Minimal Sensor Separation

From equations (15) and (17), one can compute the sensor placement for a given individual or differential SNR, and for given motion features $\overline{\omega^4}$ and $\overline{\alpha^2}$.

First, the individual SNR is above 0 dB for all values of the sensor separation, if the noise standard deviation respects

the condition $\sigma < \frac{g}{\sqrt{2}}$ (equation 15) which is fulfilled in practice as σ is close to $0.01\% g$. Figure 3 (a) shows individual SNR values above 40 dB, so the choice of the sensor separation is mainly driven by the differential SNR. The second accelerometer is considered fixed at ℓ_2 and this section studies the placement of the first location $\ell_1 = \ell_2 - d$ with $d \in \mathcal{R}^+$ the sensor separation.

As we have shown in section II-D2, the differential SNR is at its highest when the distance is maximum, which means the accelerometers are at each extremity of the limb (e.g. elbow and wrist). As a result, there is a compromise between the differential signal quality and the size of the dual-accelerometer system. For a chosen minimal SNR_δ value in equation 17, the corresponding minimal sensor separation reads:

$$d = \frac{2\sigma\sqrt{SNR_\delta}}{\sqrt{\overline{\omega^4} + \overline{\alpha^2}}} \tag{18}$$

Note that if $\overline{\omega^4} + \overline{\alpha^2} = 0$, the body segment is static and one accelerometer is needed to compute its angle.

B. Case of a Sinusoidal Motion

The limb angles during gait can be approximated by a sinusoidal function of time:

$$\phi_t = A\sin(2\pi f t) + \phi_0 \tag{19}$$

with $A \in \mathbb{R}^*$ the motion amplitude, $f \in \mathbb{R}_+^*$ the motion frequency and ϕ_0 the angle at time 0. The motion features $\overline{\omega^4}$ and $\overline{\alpha^2}$ are computed on the interval $\left[0; T = \frac{1}{f}\right]$, giving $\overline{\omega^4} = 6(\pi f A)^4$ and $\overline{\alpha^2} = 8(\pi f)^4 A^2$. Notice that, as the energy of the accelerometer signal is not defined, the SNR is defined using the average power instead of the energy:

$$SNR_\delta = (4A^2 + 3A^4)(\pi f)^4 \frac{(\ell_2 - \ell_1)^2}{2\sigma^2} \tag{20}$$

The sensor separation to get a given value of the differential SNR is then:

$$d = \frac{\sigma\sqrt{2SNR_\delta}}{(\pi f)^2 |A|\sqrt{3A^2 + 4}} \tag{21}$$

If a motion is approximated by a sinusoidal, knowing the amplitude and the frequency of this motion allows choosing a suitable sensor separation to obtain a specific differential SNR.

V. ESTIMATION OF MINIMAL SENSOR SEPARATION

In this section, we estimate the minimal sensor separation between accelerometers worn on the arm or leg, in order to achieve $SNR_\delta = 0$ dB. This value indicates that the power of differential signal and noise are equal, and is taken as a suggested limit of acceptable SNR_δ for a practical system.

A. Data Processing

Using the same three datasets, the minimal separations for a differential SNR above 0 dB are computed using equation 18, for a noise standard deviation $\sigma = 6$ mg. Results are given in Tables II, III and IV.

TABLE II

Estimated Minimal Sensor Separations for a Reaching Arm Motion. Average Angular Velocity $\overline{\omega}$ and Average Angular Acceleration $\overline{\alpha}$ Are Provided by [16]

Speed	Amplitude [deg]	$\overline{\omega}$ [rad/s]	$\overline{\alpha}$ [rad/s^2]	$\overline{\omega^4}$ [s^{-4}]	$\overline{\alpha^2}$ [s^{-4}]	d [mm]
Slow	20	0.397	0.501	0.0249	0.251	224
	30	0.537	0.613	0.083	0.375	174
	40	0.651	0.658	0.179	0.433	150
	50	0.761	0.726	0.335	0.527	127
	60	0.857	0.714	0.539	0.51	115
Intermediate	20	0.628	1.26	0.155	1.58	89.4
	30	0.85	1.53	0.521	2.34	69.6
	40	1.11	1.94	1.53	3.77	51.1
	50	1.28	2.02	2.66	4.07	45.4
	60	1.51	2.36	5.16	5.57	35.9
Ballistic	20	2.12	12.6	20.4	158	8.81
	30	2.78	16	59.5	255	6.64
	40	3.31	17.2	120	296	5.77
	50	3.9	19.2	231	368	4.81
	60	4.38	20.1	367	404	4.24

TABLE III

Estimated Minimal Sensor Separations for Arm and Leg Motion During Walking and Running, in a Laboratory Environment

Motion	Location	$\overline{\omega^4}$ [s^{-4}]	$\overline{\alpha^2}$ [s^{-4}]	d Eq. 18 [mm]	$\widehat{A}$ [deg]	$\widehat{f_0}$ [Hz]	d Eq. 21 [mm]
Walking	Upper Arm	0.398	18.3	27.2	14	0.761	29.2
Walking	Forearm	2.01	41.2	17.9	9.71	0.761	42.5
Walking	Thigh	4.08	101	11.5	42.2	0.772	8.09
Walking	Shank	85.5	497	4.88	74.3	0.772	3.63
Running	Upper Arm	62.6	665	4.36	75.9	1.37	1.11
Running	Forearm	83.7	630	4.41	78.9	1.37	1.05
Running	Thigh	23	637	4.58	76.1	1.37	1.11
Running	Shank	465	2824	2.05	78.2	1.37	1.06

TABLE IV

Estimated Distances for Walking and for Activities of Daily Life in a Residential Environment, Using the Opportunity Dataset [17]. Locations: L/R: Left/Right, L/U: Lower/Upper

Motion / Activity	Location	$\overline{\omega^4}$ [s^{-4}]	$\overline{\alpha^2}$ [s^{-4}]	d [mm]	Activity	Location	$\overline{\omega^4}$ [s^{-4}]	$\overline{\alpha^2}$ [s^{-4}]	d [mm]
Walking	RU arm	6.25	27.1	20.4	Early morning	RU arm	4.6	29.3	20.2
	RL arm	12.3	45.1	15.5		RL arm	12.5	51.7	14.7
	LU arm	4.41	28.2	20.6		LU arm	3.49	34.4	19.1
	LL arm	7.89	48.8	15.6		LL arm	5.82	58	14.7
Relaxing	RU arm	2.12	13.3	30	Clean up	RU arm	8.69	37.4	17.3
	RL arm	3.15	21.5	23.7		RL arm	24.2	67.1	12.3
	LU arm	1.52	13.1	30.8		LU arm	2.98	17.7	25.9
	LL arm	2.61	20.3	24.6		LL arm	10.5	43.5	16
Coffee time	RU arm	1.55	8.44	37.2	Sandwich time	RU arm	1.36	12.1	32.1
	RL arm	2.52	18.6	25.6		RL arm	3.64	24.6	22.1
	LU arm	1.37	7.69	39.1		LU arm	1.2	9.65	35.7
	LL arm	2.87	15.2	27.7		LL arm	3.3	21.1	23.8

During locomotion, the arm and leg motions can be approximated by a sinusoidal. In the case of the controlled locomotion experiment (III-B), the angle of each sensor relative to the vertical was computed from accelerometer data in the sagittal plane, using an arctangent function. The average motion amplitude was estimated from the angle. The fundamental frequency was estimated as the non-null frequency with the highest amplitude in the FFT power spectrum of the angle. Results are given in Table III. These features allow to compare minimal separation from equations 18 and 21.

B. Arm Motion to Reach a Target

This section focusses on the arm motion for reaching a target and the corresponding minimal separations. Results are
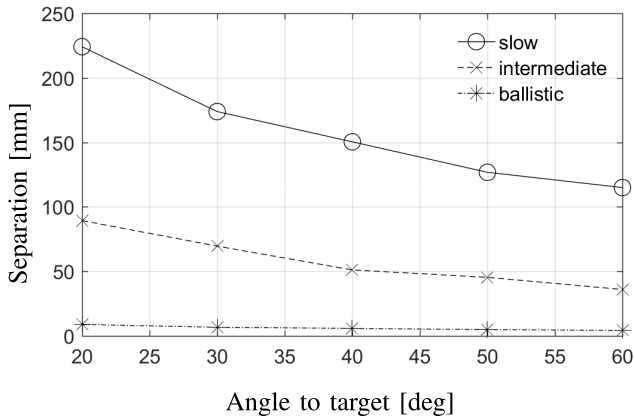
Fig. 5. Estimated minimal sensor separation for reaching arm motion as a function of the angle of the target.

given in Table II and Fig. 5. As expected, if the speed of motion increases, the minimal separation decreases, with a maximal distance of 9 mm in the ballistic case, 89 mm in the intermediate case and 224 mm in the slow case. As the amplitude increases, the average velocity and acceleration also increase so the distance decreases. For instance, the minimal distance for an intermediate speed varies from 36 to 89 mm. Therefore, there are strong variations of the minimal distance over the fifteen cases. In practice, activities of daily living are likely to be processed at an intermediate speed, or a slower speed for older people.

C. Arms and Legs During Locomotion

Tables III and IV detail the estimated minimal separation for walking and running in a laboratory environment, and walking in a residential environment. Both datasets are complementary, as the controlled locomotion dataset, collected for the study, provides reliable averages computed on long durations while the Opportunity dataset highlights natural walking speeds.

According to equation 18, the minimal separation for walking analysis in a laboratory environment is smaller on the forearm (18 mm) than on the upper arm (27 mm). It is logical as the forearm inertial data contain the forearm acceleration on top of the accelerations of the whole body and of the upper arm. For the same reason, the minimal separation is smaller on the shank (5 mm) than on the thigh (12 mm). Note that the leg distances are smaller than the arm distances because their motions have a bigger amplitude. Distances for running are even smaller (less than 5 mm) because the running motion is faster.

The estimated fundamental frequencies are close to 0.8 Hz for walking and 1.4 Hz for running. These values are consistent with the interval [0; 2] Hz indicated by [20] for angular sway, and [0.6; 5] indicated by [21] for gait pattern. In comparison with the first distances, the minimal distances computed with equation 21 are underestimated, because the sinusoidal approximation overestimates the energy of the signals. This model should be used with caution.

According to Table III, a distance of 3 cm allows to get a differential SNR greater than 0 dB for all sensor locations on

the body, for both walking and running analysis in a laboratory environment.

Results of Table IV for walking are consistent with previous comments. The minimal separation for walking is close to 20 mm on the upper arm, and 16 mm on the forearm, both sides being very similar. Separations are slightly shorter because natural walking may be less regular and induce higher angular velocity and accelerations.

D. Activities of Daily Life

In the daily life, activities are composed of mixtures of locomotion and targeted motions such as reaching. The Opportunity dataset [17] was used to estimate some typical minimal separating distances for a variety of arm motions in the context of daily activities (see Table IV). Overall, the slowest activities are 'coffee time' with an average estimated distance of 26 mm on the forearm, 'relaxing' with 24 mm and 'sandwich time' with 23 mm. During these three activities, the subject's body is on the whole static. On the contrary, 'early morning' and 'clean up' are more energetic activities and their estimated minimal distances are close to 14 mm on average on the forearm.

Similarly to results about locomotion, estimated distances are slightly shorter on forearms than on upper arms because measured accelerations are higher. The difference between the corresponding estimated distances varies from 5 to 12 mm. The highest differences are found for activities 'coffee time' and 'sandwich time' which involve motions such as bringing a cup or a sandwich to the mouth, moving mainly forearms.

Estimated distances in the Table IV are overall very similar for both arms, in particular for 'relaxing' and 'early morning'. However, it is interesting to note that for some activities such as 'coffee time', 'clean up' and 'sandwich time', angular velocities and accelerations are on average higher on the right side, resulting in slightly shorter minimal distances. This may be due to the fact that subjects were probably right-handed. The difference between distances on both sides stays below 1 cm and choosing the largest distance ensures a good SNR on both sides. On the opposite, wearing a dual-accelerometer on the dominant hand allows a more compact system for a given SNR.

VI. CONCLUSION

This paper studied the performance of a dual-accelerometer system, in particular the novel analysis of the quality of the differential signal, depending on the sensor configuration.

Based on a 2D kinematic model of body segments and a statistical model of measurements, the individual and differential Signal-to-Noise-Ratios (SNR) were analytically defined to quantify signal quality. They depend on the sensor placement and separation, the noise standard deviation and two motion features. These SNR were estimated for three datasets: the Nagasaki dataset for arm motion profiles [16], the Controlled Locomotion dataset collected for this study for locomotion on a treadmill, and the Opportunity dataset [17] activities of daily life. While the individual SNR is very high in practice, we show it is possible to achieve a good differential

SNR if the sensor placement and separation are well chosen. So, one can choose a minimal sensor separation to reach a given differential SNR. The estimated minimal separations computed for differential SNR value of 0 dB and a noise of 6 mg, were discussed for reaching, walking and running, and activities of daily life. A distance of 3 cm ensures a differential SNR greater than 0 dB on arms and legs during reaching, walking and running, both in a laboratory or in a residential environment. This distance is also appropriate to measure arm motions during most activities of the Opportunity dataset. Such distances, computed for a noise of 6 mg, increase linearly with the noise standard deviation.

The minimal differential SNR chosen for the estimation of sensor separations should be sufficient for classification analysis and kinematic estimation. However, as the paper provided motion features for all motions and activities studied, minimal distances can easily be recalculated with equations 17 or 21 for any level of differential SNR required, in the limit of the body segment length. If the target user group has mixed functional capacity, we suggest to identify the sensor separation which guarantees a sufficient SNR in all cases. Ultimately the power requirements for gyroscopes may make them more attractive for long term wearable sensors, but in the interim these metrics will enable a quantified basis for any design decisions for wearable technologies.

REFERENCES

[1] A. Godfrey, R. Conway, D. Meagher, and G. ÓLaighin, "Direct measurement of human movement by accelerometry," *Med. Eng. Phys.*, vol. 30, no. 10, pp. 1364–1386, Dec. 2008.

[2] K. Liu, T. Liu, K. Shibata, Y. Inoue, and R. Zheng, "Novel approach to ambulatory assessment of human segmental orientation on a wearable sensor system," *J. Biomech.*, vol. 42, no. 16, pp. 2747–2752, Dec. 2009.

[3] A. T. M. Willemsen, C. Frigo, and H. B. K. Boom, "Lower extremity angle measurement with accelerometers-error and sensitivity analysis," *IEEE Trans. Biomed. Eng.*, vol. 38, no. 12, pp. 1186–1193, Dec. 1991.

[4] R. Takeda, S. Tadano, M. Todoh, M. Morikawa, M. Nakayasu, and S. Yoshinari, "Gait analysis using gravitational acceleration measured by wearable sensors," *J. Biomech.*, vol. 42, no. 3, pp. 223–233, Feb. 2009.

[5] M. D. Djurić-Jovićić, N. Jovićić, D. Popović, and A. Djordjević, "Nonlinear optimization for drift removal in estimation of gait kinematics based on accelerometers," *J. Biomech.*, vol. 45, no. 16, pp. 2849–2854, 2012.

[6] T. Seel, J. Raisch, and T. Schauer, "IMU-based joint angle measurement for gait analysis," *Sensors*, vol. 14, no. 4, pp. 6891–6909, Jan. 2014.

[7] F. Alonge, E. Cucco, F. D'Ippolito, and A. Pulizzotto, "The use of accelerometers and gyroscopes to estimate hip and knee angles on gait analysis," *Sensors*, vol. 14, no. 5, pp. 8430–8446, Jan. 2014.

[8] V. Bonnet, C. Mazzà, P. Fraisse, and A. Cappozzo, "Real-time estimate of body kinematics during a planar squat task using a single inertial measurement unit," *IEEE Trans. Biomed. Eng.*, vol. 60, no. 7, pp. 1920–1926, Jul. 2013.

[9] J. Favre, B. M. Jolles, R. Aissaoui, and K. Aminian, "Ambulatory measurement of 3D knee joint angle," *J. Biomech.*, vol. 41, no. 5, pp. 1029–1035, Jan. 2008.

[10] E. Chalmers, J. Le, D. Sukhdeep, J. Watt, J. Andersen, and E. Lou, "Inertial sensing algorithms for long-term foot angle monitoring for assessment of idiopathic toe-walking," *Gait Posture*, vol. 39, no. 1, pp. 485–489, Jan. 2014.

[11] W. Zeng and C. Wang, "Human gait recognition via deterministic learning," *Neural Netw.*, vol. 35, pp. 92–102, Nov. 2012.

[12] V. Lugade, E. Fortune, M. Morrow, and K. Kaufman, "Validity of using tri-axial accelerometers to measure human movement—Part I: Posture and movement detection," *Med. Eng. Phys.*, vol. 36, no. 2, pp. 169–176, Feb. 2014.

[13] *Digital Output MEMS Accelerometer ADXL362*, Analog Devices, Cambridge, MA, USA, 2013.

[14] *MPU-6000 and MPU-6050 Product Specification Revision 3.4*, InvenSense Inc., San Jose, CA, USA, 2013.

[15] S. O. H. Madgwick, A. J. L. Harrison, P. M. Sharkey, R. Vaidyanathan, and W. S. Harwin, "Measuring motion with kinematically redundant accelerometer arrays: Theory, simulation and implementation," *Mechatronics*, vol. 23, no. 5, pp. 518–529, 2013.

[16] H. Nagasaki, "Asymmetric velocity and acceleration profiles of human arm movements," *Experim. Brain Res.*, vol. 74, no. 2, pp. 319–326, 1989.

[17] D. Roggen *et al.*, "Collecting complex activity datasets in highly rich networked sensor environments," in *Proc. 7th Int. Conf. IEEE Netw. Sens. Syst. (INSS)*, Kassel, Germany, Jun. 2010, pp. 233–240.

[18] M. Djuric, "Automatic recognition of gait phases from accelerations of leg segments," in *Proc. 9th IEEE Symp. Neural Netw. Appl. Elect. Eng.*, Belgrade, Serbia, Sep. 2008, pp. 121–124.

[19] P. Cheng and B. Oelmann, "Joint-angle measurement using accelerometers and gyroscopes—A survey," *IEEE Trans. Instrum. Meas*, vol. 59, no. 2, pp. 404–414, Feb. 2010.

[20] A. Caroselli, F. Bagalà, and A. Cappello, "Quasi-real time estimation of angular kinematics using single-axis accelerometers," *Sensors*, vol. 13, no. 1, pp. 918–937, Jan. 2013.

[21] B. Najafi, K. Aminian, A. Paraschiv-Ionescu, F. Loew, C. J. Bula, and P. Robert, "Ambulatory system for human motion analysis using a kinematic sensor: Monitoring of daily physical activity in the elderly," *IEEE Trans. Biomed. Eng.*, vol. 50, no. 6, pp. 711–723, Jun. 2003.

Emma Villeneuve received the master's degree in physics from the School of Engineering PHELMA, Grenoble, in 2009, the master's degree in signal and image processing from the Grenoble Institute of Technology, France, in 2009, and the Ph.D. degree in signal processing from the University of Toulouse, France, for astrophysical hyperspectral data. From 2013 to 2015, she was a Research Assistant with the University of Reading, U.K. She is currently an Associate Research Fellow with NIHR CLAHRC South West Peninsula, University of Exeter, U.K. Her research interests are in the areas of statistical signal processing, with specific focus on healthcare applications.

William Harwin is currently a Professor of Interactive Systems with the University of Reading. His research interests include technology and healthcare, human–robot interactions, and haptic interfaces. Haptics research includes the control, rendering, and applications, most recently activity was work with Kings College on the hapTEL project that explore haptics as an educational tool in dental education. He has a long standing interest in assistive and rehabilitation robotics with a specific interest in neurorehabilitation for individuals following a stroke and was a Chair of the IEEE International Conference on Rehabilitation Robotics conference series. More recent research includes healthcare sensors in a residential environment and the emerging field of cognitive robotics.

William Holderbaum received the M.Sc. degree in automatic control from the University of Reims, Reims, France, in 1993, and the Ph.D. degree from the University of Lille, Lille, France, in 1999. He was a Research Assistant with the University of Glasgow, Glasgow, U.K., from 1999 to 2001. He is currently a Professor with the School of Systems Engineering. His research interests are in control theory and its applications. These are mainly focused on rehabilitation engineering and in particular robust control for unsupported paraplegic standing. Furthermore, he has published papers in the area of geometric control theory in particular Hamiltonian systems and optimization problems.

R. Simon Sherratt (M'97–SM'02–F'12) received the B.Eng. degree in electronic systems and control engineering from Sheffield City Polytechnic, U.K., in 1992, and the M.Sc. degree in data telecommunications and the Ph.D. degree in video signal processing from the University of Salford, U.K., in 1994 and 1996, respectively. In 1996, he was appointed as a Lecturer in Electronic Engineering at the University of Reading, where he is currently a Professor of Biosensors. His research topic is signal processing and communications in consumer electronic devices focusing on wearable devices and healthcare. He received the First Place IEEE Chester Sall Memorial Award in 2006 and the Second Place Award in 2016. He is currently the Editor-in-Chief of the IEEE TRANSACTIONS ON CONSUMER ELECTRONICS and a Reviewer of the IEEE SENSORS JOURNAL on wearable sensors.

Ruth White received the M.Eng. degree in cybernetics from the University of Reading in 2012. She has spent a year working for Ultra Electronics on a variety of projects, including sonar systems. She is currently pursuing the Ph.D. degree in cybernetics with the University of Reading, as part of the SPHERE IRC project. She is looking at using the machine learning algorithm, topic models, to detect behavior patterns for healthcare monitoring.